Supplementary material for LHCb-PAPER-2014-063

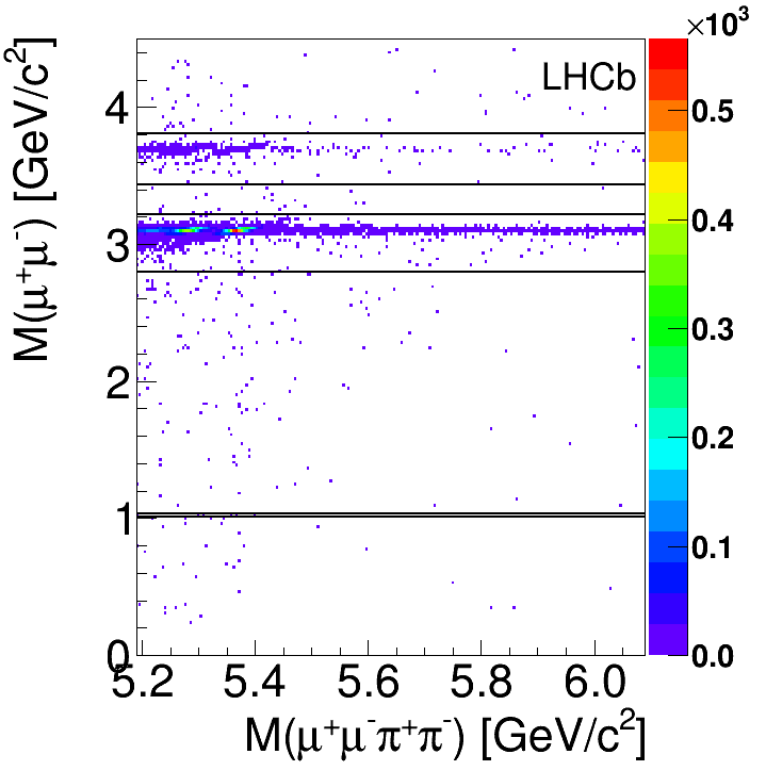

Figure 1: Distribution of the $\mu^+\mu^-$ mass versus the $\pi^+\pi^-\mu^+\mu^-$ mass, before the vetoes to remove dimuon resonances. The black lines define the regions to veto $\phi \to \mu^+\mu^-$, $J/\psi \to \mu^+\mu^-$, and $\psi(2S) \to \mu^+\mu^-$ decays; they are 1.010–1.030 GeV/c^2, 2.796–3.216 GeV/c^2, and 3.436–3.806 GeV/c^2, respectively.

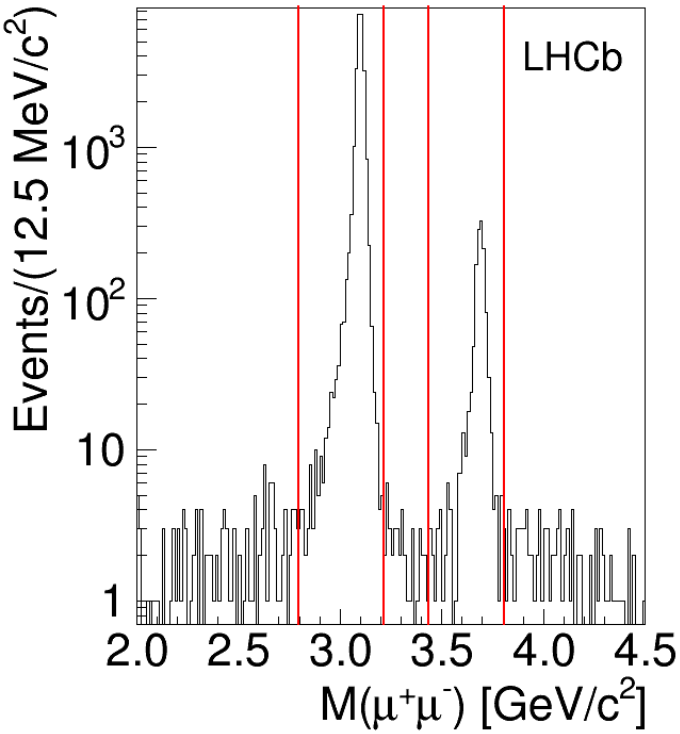

Figure 2: Distribution of the $\mu^+\mu^-$ mass in the range 2–4.5 GeV/c^2 to show the J/ψ and $\psi(2S)$ resonances with their radiative tails. All candidates with $\pi^+\pi^-\mu^+\mu^-$ invariant mass in the range 5.19–6.99 GeV/c^2 are considered. The red lines define the regions to veto $J/\psi \to \mu^+\mu^-$ and $\psi(2S) \to \mu^+\mu^-$ decays; they are 2.796–3.216 GeV/c^2 and 3.436–3.806 GeV/c^2, respectively.

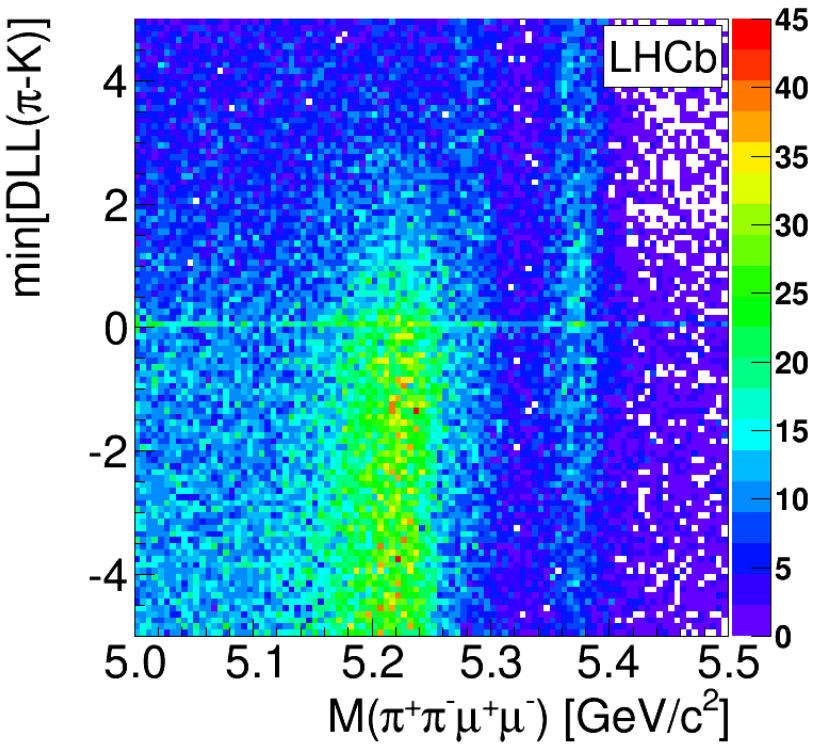

Figure 3: Distribution of the pion DLL(π-K) versus the $\pi^+\pi^-\mu^+\mu^-$ mass; for each candidate, the minimum value between the DLL(π-K) of the two pions is considered. The $B^0_{(s)} \to J/\psi\ \pi^+\pi^-$ and $B^0_{(s)} \to \pi^+\pi^-\mu^+\mu^-$ candidates are merged together. The variable DLL(π-K) is the difference of the logarithm of the likelihood of a track to be a π or a K. The accumulation of events at DLL(π-K)$= 0$ is given by particles with momentum below the Cherenkov threshold in the RICH detectors. The accumulation of candidates in the region around 5.2 GeV/c^2 for DLL(π-K)< 1 is due to $B^0 \to J/\psi\, K^*(892)^0$ and $B^0 \to K^*(892)^0\mu^+\mu^-$ decays, where the kaon is misidentified with a pion. The band around 5.37 GeV/c^2 is given by $B^0_s \to J/\psi\ \pi^+\pi^-$ and $B^0_s \to \pi^+\pi^-\mu^+\mu^-$ decays candidates; the band around 5.28 GeV/c^2 is due to $B^0 \to J/\psi\ \pi^+\pi^-$ and $B^0 \to \pi^+\pi^-\mu^+\mu^-$ decays candidates. In the analysis, the requirement DLL(π-K)> 1 is set to suppress the misidentified decays.

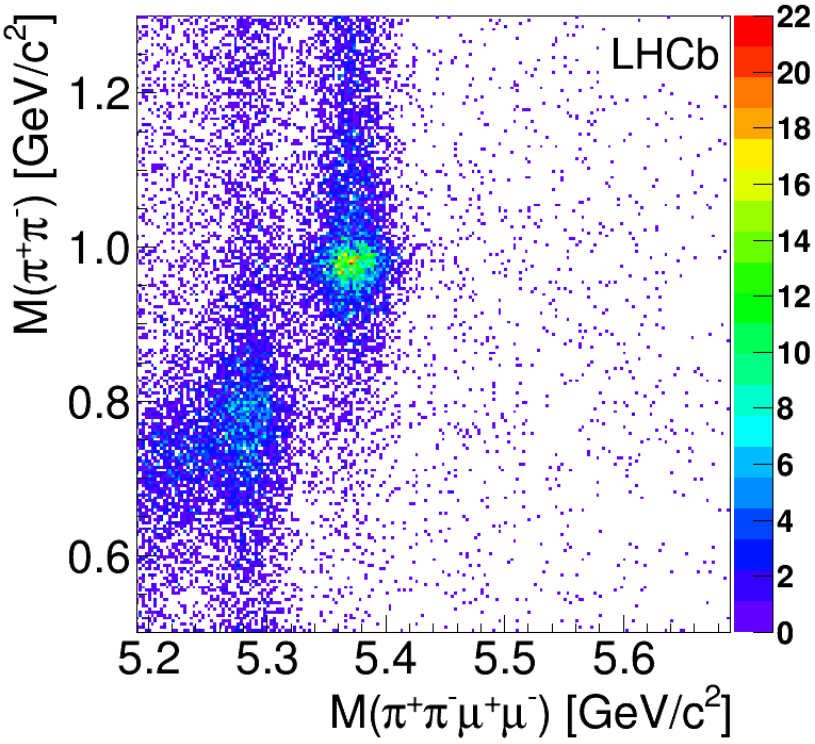

Figure 4: Distribution of the $\pi^+\pi^-$ mass versus the $\pi^+\pi^-\mu^+\mu^-$ mass. The $B^0_{(s)} \to J/\psi\, \pi^+\pi^-$ and $B^0_{(s)} \to \pi^+\pi^-\mu^+\mu^-$ candidates are merged together.

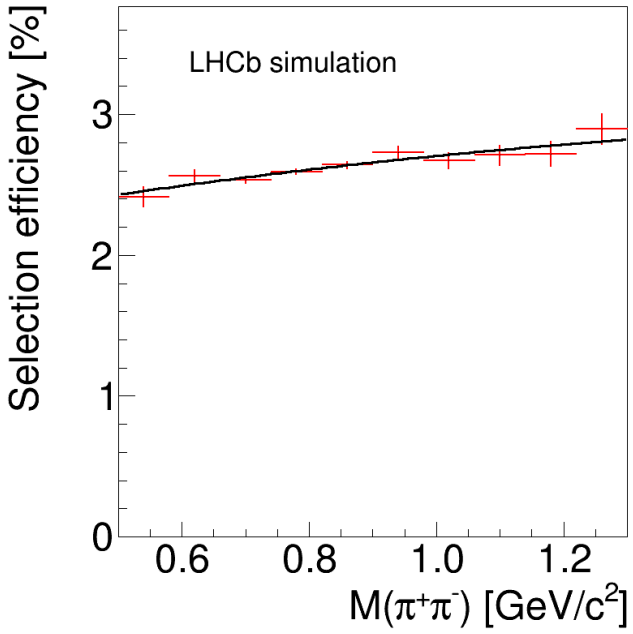

Figure 5: Selection efficiency for $B_s^0 \to \pi^+\pi^-\mu^+\mu^-$ decays as a function of the $\pi^+\pi^-$ mass for simulated events. The black curve represents the fit to the simulated data with a second-order polynomial. The variation of the efficiency is of the order of 15%.

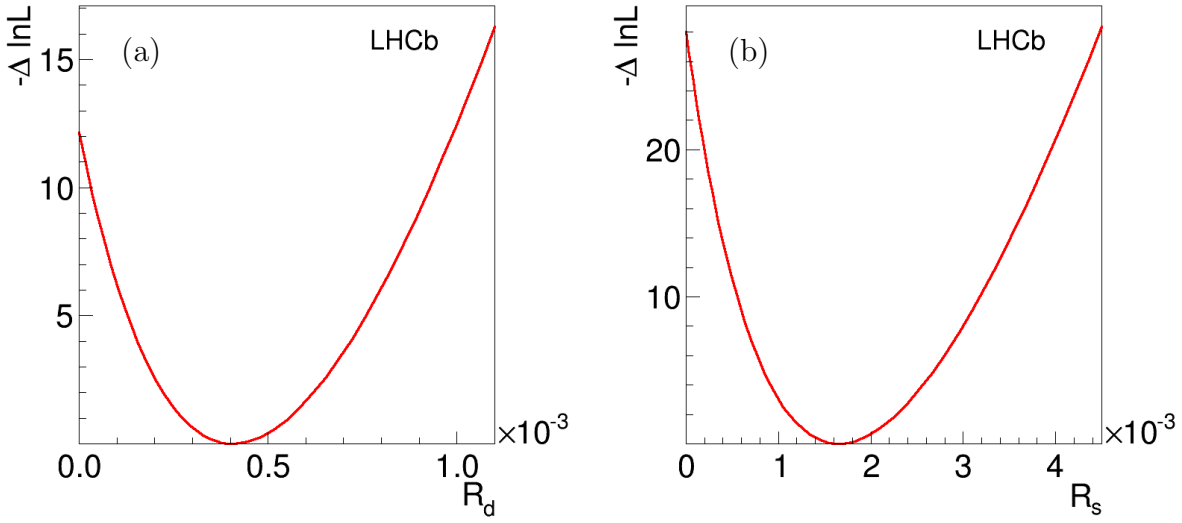

Figure 6: Likelihood profiles of (a) $\mathcal{R}_d$ and (b) $\mathcal{R}_s$. For each value of $\mathcal{R}_d$ ($\mathcal{R}_s$) probed, all other parameters are floating in the minimisation of the likelihood. Systematic uncertainties are not included.

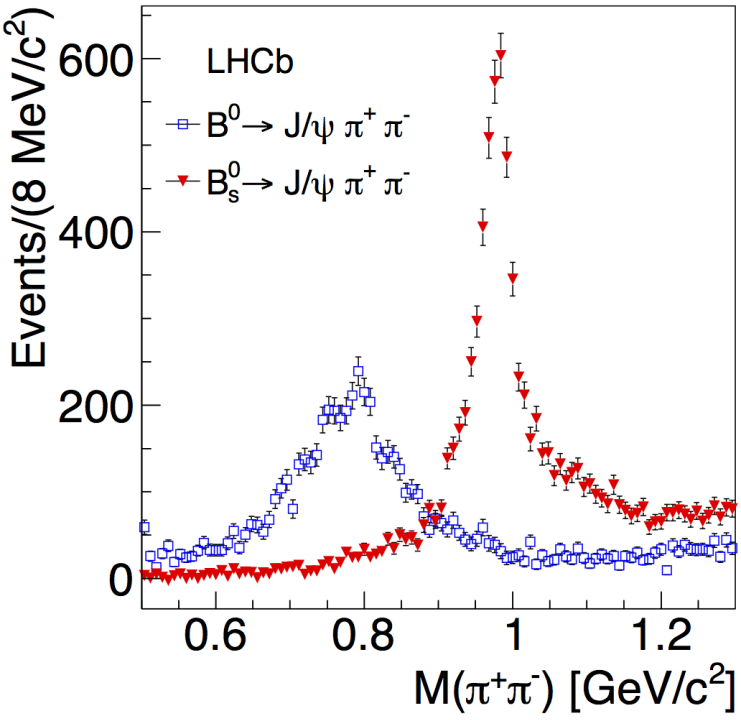

Figure 7: Background-subtracted $\pi^+\pi^-$ mass distributions of $B^0_{(s)} \to J/\psi\ \pi^+\pi^-$ candidates.